# Electrochemical ageing study of mixed lanthanum/praseodymium nickelates La2-PrNiO4+$\delta$ as oxygen electrodes for solid oxide fuel or electrolysis cells

Vaibhav Vibhu, Aurelien Flura, Aline Rougier, Clément Nicollet, Sébastien Fourcade, Teresa Hungría, Jean-Claude Grenier, Jean-Marc. Bassat

# Electrochemical ageing study of mixed lanthanum/praseodymium nickelates $La_{2-x}Pr_xNiO_{4+\delta}$ as oxygen electrodes for solid oxide fuel or electrolysis cells

Vaibhav Vibhu[a], Aurélien Flura[a], Aline Rougier[a], Clément Nicollet[a], Sébastien Fourcade[a], Teresa Hungria[b], Jean-Claude Grenier[a], Jean-Marc Bassat[a,*]

[a]*CNRS, Univ. Bordeaux, Bordeaux INP, ICMCB, UMR 5026, F-33600 Pessac Cedex, France*

[b] *Centre de Microcaractérisation Raimond CASTAING, Université de Toulouse, CNRS, UT3 – Paul Sabatier, INP, INSA, Espace Clément Ader, 3 rue Caroline Aigle, 31400 TOULOUSE France*

*Corresponding author. E-mail address: jean-marc.bassat@icmcb.cnrs.fr (J.-M. Bassat).

**Abstract:** The chemical and electrochemical stability of lanthanide nickelates $La_2NiO_{4+\delta}$ (LNO), $Pr_2NiO_{4+\delta}$ (PNO) and their mixed compounds $La_{2-x}Pr_xNiO_{4+\delta}$ (LPNOs) with $x$ = 0.5, 1 or 1.5 is reported. The aim is to promote these materials as efficient electrodes for solid oxide fuel cell (SOFC) and/or solid oxide electrolysis cell (SOEC). $La_2NiO_{4+\delta}$ and $La_{1.5}Pr_{0.5}NiO_{4+\delta}$ compounds are chemically very stable as powders over one month in the temperature range 600 – 800 °C, while the other materials rich in praseodymium progressively decompose into various perovskite-deriving components with additional $Pr_6O_{11}$. Despite their uneven properties, all these materials are quite efficient and sustainable as electrodes on top of gadolinium doped ceria ($GDC_{BL}$) // yttrium doped zirconia (8YSZ) electrolyte, for one month at 700 °C without polarization. Under polarization (300 $mA \cdot cm^{-2}$), the electrochemical performances of LNO, PNO and $La_{1.5}Pr_{0.5}NiO_{4+\delta}$ (LP5NO) quickly degrade in SOFC mode, i.e. for the oxygen reduction reaction, while they show durability in SOEC mode, i.e. for the oxide oxidation reaction.

Keywords: Lanthanide nickelates; SOFC cathode; SOEC anode; Ageing; Degradation

## 1. Introduction

The reduction of the operating temperature of Solid Oxide Fuel Cells (SOFCs) or Solid Oxide Electrolysis Cells (SOECs) is a critical challenge for their commercialization. Presently, the objective is to decrease it down to the intermediate range (600 – 700 °C), with the aim to reduce the cost by using stainless steel instead of ceramics as interconnects for instance, as well as to improve their long-term cell durability. In this scope, the study of the long-term stability of the SOFC ceramic components is paramount [1, 2]. The cell degradation is generally due to various phenomena such as, i) a grain coarsening, particle smoothing/rounding and/or phase instability occurring at the electrodes, ii) an interfacial segregation, impurities accumulation and cationic inter-diffusions occurring at the interfaces between the different layers of the cell.

As the oxygen electrode contributes to a large extent to the cell polarization resistance, $R_p$, a lot of work available in the literature aims to design materials with MIEC properties [3-6] suitable for both SOFCs and SOECs. In this respect oxygen deficient perovskites based materials have been extensively studied e.g. $La_{1-x}Sr_xCo_{1-y}Fe_yO_{3-\delta}$ (LSCF) [7-10], $La_{1-x}Sr_xCoO_{3-\delta}$ (LSC) [11-13], $Ba_{1-x}Sr_xCo_{1-y}FeyO_{3-\delta}$ (BSCF) [14, 15]. However these La, Sr-cobaltites based oxygen electrode materials have inherent disadvantages: (a) a Sr-segregation leading to the formation of $SrZrO_3$ insulating phase [16-19]; (b) high values of thermal expansion coefficients [4, 5] and (c) a crystallographic phase transition from rhombohedral to cubic [20], leading to a degradation of the cell performances. Ba, Sr-cobaltites based oxygen materials also exhibit a poor chemical stability [21].

More recently, another kind of MIEC oxides having the $K_2NiF_4$-type layered structure and showing oxygen over-stoichiometry (instead of oxygen vacancies in the previous perovskite-type materials)

has been reported as oxygen electrode materials. For example, rare earth nickelates $Ln_2NiO_{4+\delta}$ (Ln = La or Pr) have been studied from long time [22-24]. Indeed, these compounds show good electronic conductivity [25, 26] and high diffusivity of oxide ions [27-29]. Then, due to their large anionic bulk diffusion ($D^*$) as well as surface exchange coefficients ($k^*$), combined with good electrical conductivity and thermal expansion properties matching with those of electrolyte materials, they have been extensively used as oxygen electrodes in Solid Oxide Cells [30-35]. Among these nickelates, PNO shows the lowest polarization resistance ($R_p$) [32] while LNO is highly chemically stable [36]. In a recent study, lanthanum praseodymium nickelates $La_{2-x}Pr_xNiO_{4+\delta}$ ($0.0 \leq x \leq 2.0$) (hereafter labeled LPNO) were considered to find the best compromise between high electrochemical performance and long-term chemical stability [37]. The electrochemical performance in these mixed La, Pr-nickelates is increased with increasing Pr-content. For instance, a $R_p$ value of 0.93 Ω·cm² is achieved at 600 °C for LNO/GDC/8YSZ symmetrical cell while after substitution of La by Pr, the $R_p$ values decrease down to 0.37, 0.29, 0.23 and 0.15 Ω·cm² for $La_{1.5}Pr_{0.5}NiO_{4+\delta}$, $LaPrNiO_{4+\delta}$, $La_{0.5}Pr_{1.5}NiO_{4+\delta}$ and PNO, respectively.

Regarding single cell performances, the PNO electrode containing single cell shows better behavior than LSCF electrode deposited on the same Ni-YSZ/YSZ/GDC support, in both SOFC and SOEC mode. The corresponding LNO single cell has lower performance than LSCF cell in SOFC mode while almost comparable behavior than LSCF in SOEC mode [38]. Kim et al. have also reported similar results for LNO [39].

The next step is to prove the durability of these nickelates based cells over the long term. In this paper, ageing of LNO, PNO and LPNO without polarization for one month or under $i_{dc}$ = 300 mA·cm$^{-2}$ for two-and-a-half month is reported. In the latter case, the results of the ageing are given for the electrode operating in SOFC mode, i.e. the reduction of $O_2$, or in high-temperature electrolysis (SOEC) mode, i.e. the oxidation of $O_2$.

The degradation occurring during the ageing is analysed and discussed based on X-ray diffraction and FIB-SEM analysis.

## 2. Experimental

### *2.1. Powder preparation*

Five compositions of $La_{2-x}Pr_xNiO_{4+\delta}$, with $x$ = 0.0 (LNO), 0.5 (LP5NO), 1.0 (LP10NO), 1.5 (LP15NO), or 2.0 (PNO) were synthesized using the citrate-nitrate route (modified Pechini method) [40]. The corresponding precursors were $Pr_6O_{11}$ (Aldrich chem, 99.9%), $La_2O_3$ (Strem Chemical, 99.99%) and $Ni(NO_3)_2{\cdot}6H_2O$ (Acros Organics, 99%). The final annealing was performed at 1200 °C for 12 h under air, leading to single and well-crystallized phases for all compositions. The resulting powders were attrited using zirconia balls and ethanol for 4 h to reach an average particle size of about 0.6 µm. More details about the powder preparation are given in ref. [37].

### *2.2.Cell manufacturing*

Symmetrical half-cells (LPNO electrode//$GDC_{BL}$//8YSZ) were shaped for the electrochemical studies. Terpineol-based inks were prepared for the different LPNO phases and the 20 at.% gadolinium doped ceria barrier layer ($GDC_{BL}$). First, $GDC_{BL}$ layers (thickness ≈ 3 µm) were symmetrically screen printed on both sides of dense 8YSZ pellets (diameter ≈ 18 mm and thickness ≈ 1.2 mm), then sintered at 1300 °C, for 1 h, in air. The nickelate layers (thickness ≈ 10–15 µm, ∅ ~ 15 mm) were afterwards symmetrically screen printed and sintered at 1150 °C, for 1 h, under $N_2$ atmosphere ($p_{O2} \approx 10^{-4}$ atm), then re-oxidized under air at 800 °C in the set-up. These sintering temperatures were previously optimized to obtain a controlled homogeneous porous electrode microstructure corresponding to the lowest polarization resistance $R_p$ values recorded for these materials [37, 41].

*2.3.Electrochemical characterization*

Electrochemical measurements, as well as ageing experiments, were performed using symmetrical half-cells as described in Fig. 1. Two geometries were considered:

(i) a symmetric two electrodes system for experiments without polarization; in that case, only the potential $U_{total}$ is measured to obtain the impedance diagrams.

(ii) a so-called "three-electrode" system for the ageing under polarization ($i_{dc}$ = 300 mA·cm$^{-2}$): a reference electrode is needed in that case, which is a painted ring of platinum set all around the edge of the thick 8YSZ electrolyte ceramic, in a region of stable potential [42-44]. Under a given polarization, the electrodes differently behave depending on the current flow going through them: then, one electrode works in SOFC mode characterized by $U_{SOFC}$, the second one works in SOEC mode characterized by $U_{SOEC}$, the whole cell being characterized using $U_{total}$.

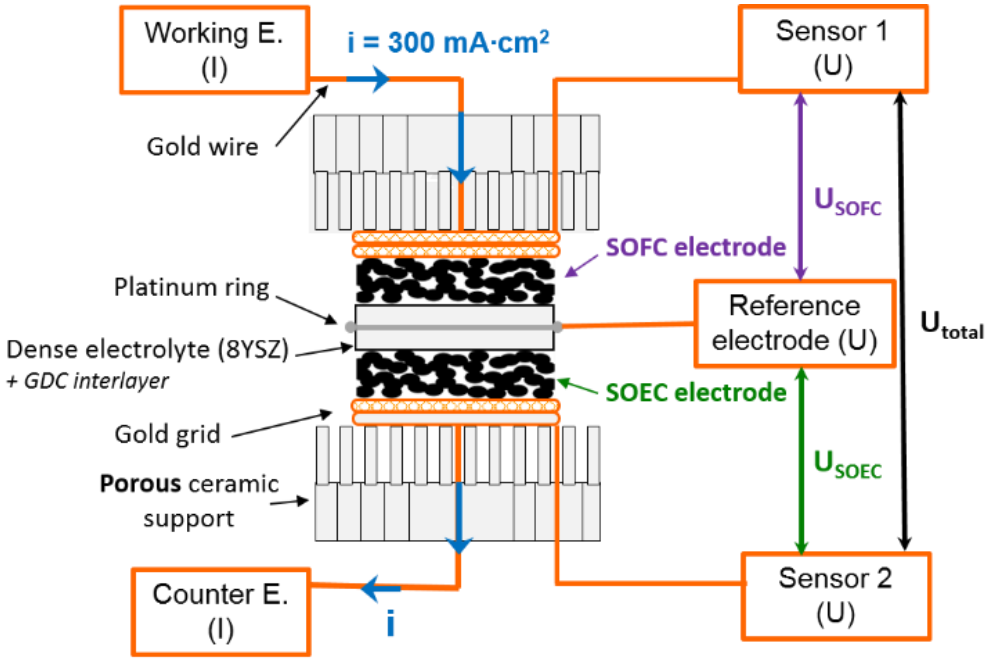


**Fig. 1.** EIS setup describing the three electrodes measurement configuration.

Current collectors were made of gold grids (1024 meshes per $cm^2$). All the EIS measurements, either on as-prepared or aged cells, were always carried out in air, in the temperature range 500–800 °C. The impedance diagrams were recorded at steady state ($i_{dc}$ = 0 $mA \cdot cm^{-2}$), under potentiostatic control with 50 mV ac amplitude, from $10^6$ Hz down to $10^{-1}$ Hz, using a frequency response analyzer Autolab FRA2, coupled with a potentiostat/galvanostat PGSTAT 302N. For the ageing study under polarization, EIS measurements were performed every few hours; the *d*c current was stopped and the cell stabilized for 10 min, prior to the EIS measurements. The complex impedance diagrams were fitted using Zview2® (Scribner associates, inc.). The polarization resistance $R_p$ was calculated from the difference between the low (LF) and the high frequencies (HF) diagram intercepts with the $Z'$-axis of the Nyquist representation, and the $R_s$ (series resistance) values were obtained by taking the high-frequency intercept on $Z'$-axis.

### *2.4. XRD analyses*

All the X-ray diffraction analyses for the LPNOs raw powders and the thermally aged powders were performed using a PAN-analytical X'pert MPD diffractometer with Cu-$K_\alpha$ ($\lambda$ = 0.15418 nm) incident radiation. The ageing of the powders was conducted as follows: three green pellets (about 60% density) were first prepared and then left in air, for one month, at 800 °C (the EIS measurement temperature) and at 700 °C and 600 °C , before being crushed into powders prior to the XRD characterization.

The top surfaces of the LNPO electrodes screen-printed on $GDC_{BL}$//8YSZ were also analyzed, after the ageing processes at 700 °C under $i_{dc}$ = 300 $mA \cdot cm^{-2}$.

### *2.5. FIB-SEM analyses*

Cross sections of aged cells were prepared by focused ion beam milling; subsequent SEM images and elemental microanalyses were recorded using a Dual Beam SEM / FIB FEI Helios 600i equipped with an EDX Oxford Instruments analyser Aztec Advanced equipped with a SDD detector.

## 3. Results

Before studying the ageing of the materials as electrode on $GDC_{BL}$//8YSZ, it was necessary to determine their chemical stability as raw powder.

### *3.1. Chemical stability of LNO, PNO and LPNOs for one month at T = 600 °C, 700 °C or 800 °C*

The short-term chemical stability of LNO ($x = 0$) and PNO ($x = 1$) has been previously reported by our group [45]. In the current study, we verified that LNO is chemically stable up to one month, whatever the temperature. PNO decomposes at 600 °C into $Pr_6O_{11}$ and $PrNiO_{3-\delta}$, and at 700 °C and 800 °C with additional $Pr_4Ni_3O_{10+\delta}$. This behaviour agrees with another of our recent article [46] reporting that $PrNiO_{3-\delta}$ decomposes into $Pr_4Ni_3O_{10+\delta}$ at $T \geq 700$ °C in air.

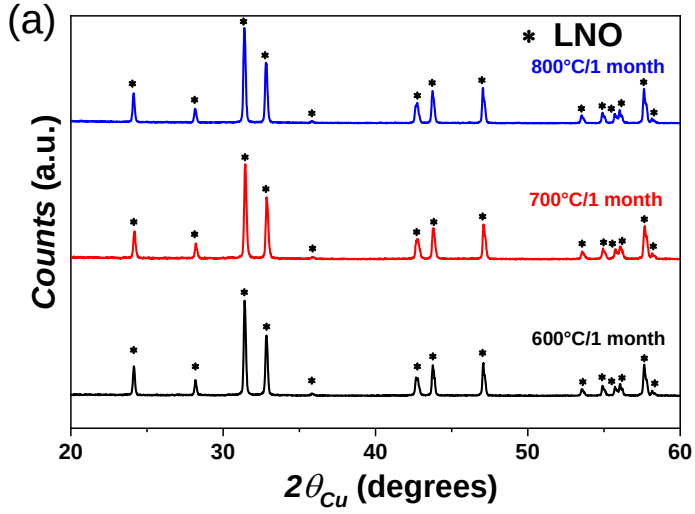

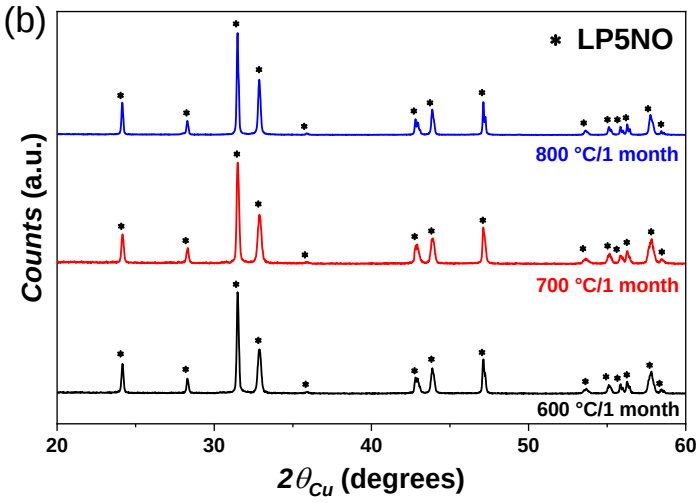
(b)
* LP5NO
800 °C/1 month
700 °C/1 month
600 °C/1 month
Counts (a.u.)
20
30
40
50
60
2θCu (degrees)

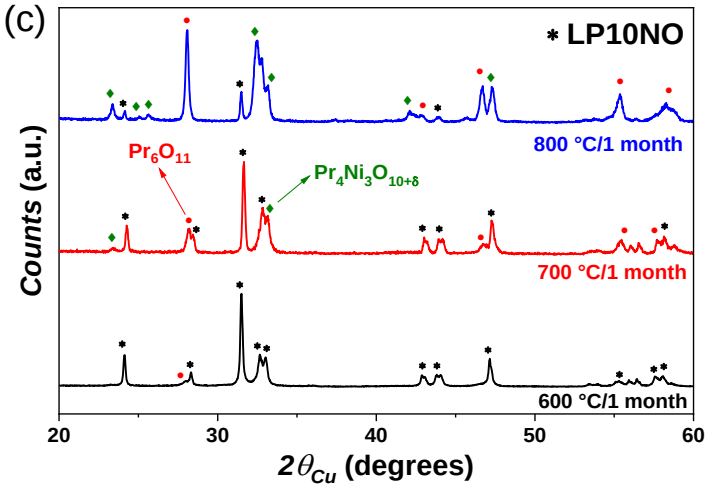
(c)
* LP10NO
800 °C/1 month
Pr6O11
Pr4Ni3O10+δ
700 °C/1 month
600 °C/1 month
Counts (a.u.)
20
30
40
50
60
2θCu (degrees)

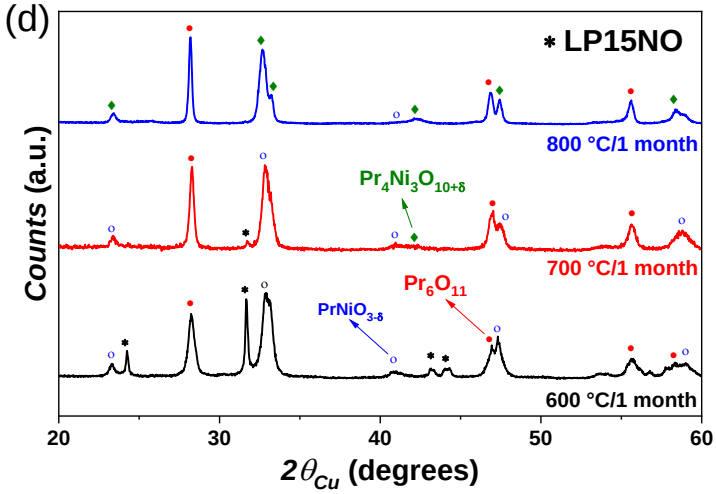
(d)
* LP15NO
800 °C/1 month
Pr4Ni3O10+δ
700 °C/1 month
Pr6O11
PrNiO3-δ
600 °C/1 month
Counts (a.u.)
20
30
40
50
60
2θCu (degrees)

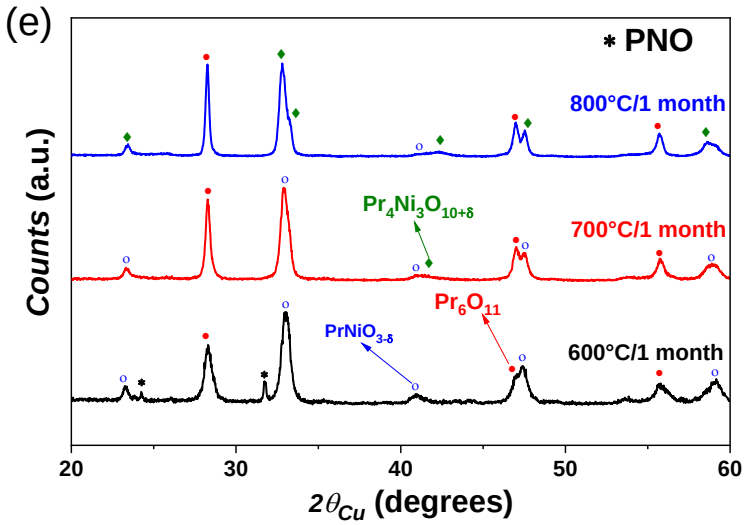


Fig. 2. X-ray diffractograms of $La_{2-x}Pr_xNiO_{4+\delta}$ for $x$ = (a) 0 (LNO), (b) 0.5 (LP5NO), (c) 1 (LP10NO), and (d) 1.5 (LP15NO) and (e) 2 (PNO) after ageing one month at $T$ = 600 °C, 700 °C and 800 °C.

The XRD results recorded for LP5NO, LP10NO and LP15NO are reported in Fig. 2. The compounds with high contents of praseodymium (LP10NO and LP15NO) are chemically unstable and undergo the same decomposition behaviour than PNO. The compound with the highest content of lanthanum (LP5NO) is chemically stable, as its parent phase LNO.

### *3.2. Electrochemical stability of LNO, PNO and LPNOs*

#### *3.2.1. Electrochemical stability for one month at 700 °C without polarization ($i_{dc}$ = 0 mA·cm$^{-2}$)*

The polarization resistances $R_p$ of LNO, PNO and LPNOs electrodes supported on $GDC_{BL}$//8YSZ electrolyte were measured after one month ageing at 700 °C, without polarization ($i_{dc}$ = 0 mA·cm$^{-2}$).

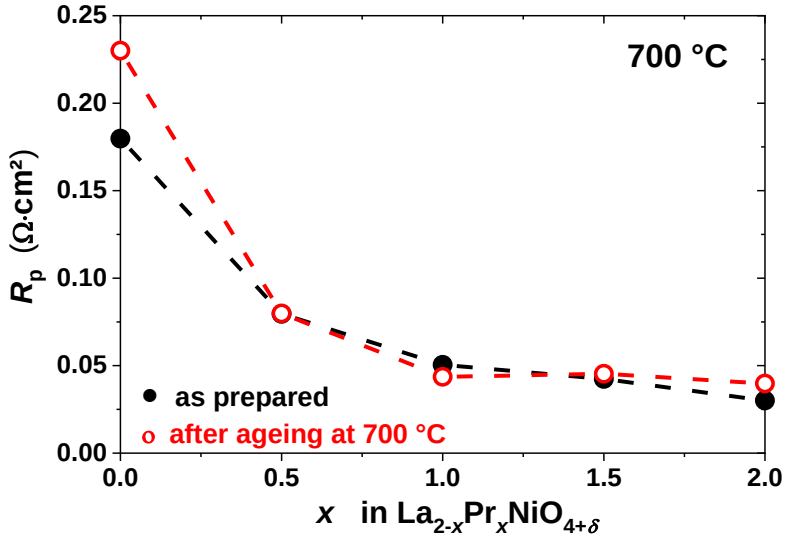


Fig. 3. Composition dependence of the polarization resistance $R_p$ of LPNO compounds as-prepared and after one month at 700 °C without polarization.

The results reported in Fig. 3 show that the polarization resistances of the parent phases LNO and PNO slightly increase, it is even much more pronounced for LNO. This result is surprising concerning LNO since the material is chemically stable in these conditions; a progressive reactivity at its interface with the $GDC_{BL}$//YSZ electrolyte might explain this degradation [47]. For the LPNO compounds, no clear variation can be observed, LP10NO exhibiting even better performances after one month.

### *3.2.2. Electrochemical behaviour of LNO, PNO and LP5NO for one month at 700 °C under polarization*

The electrochemical impedance spectroscopy data of PNO, LNO, and $La_{1.5}Pr_{0.5}NiO_{4+\delta}$ (LP5NO) were recorded over two-and-a-half months (i.e. 1800 hrs) at 700 °C, under polarization ($i_{dc}$ = 300 mA·cm$^{-2}$). LP5NO was selected with regard to its good long-term chemical stability (cf. Fig. 2b).

The results for PNO are reported in Fig. 4, the electrode operating either in SOEC or SOFC conditions. In SOEC mode, inductive loops clearly appear; they are well-known measurement artifacts when using three-electrode setup [42-44, 48, 49]. Such inductive loops can be accurately fitted using a negative R//CPE.

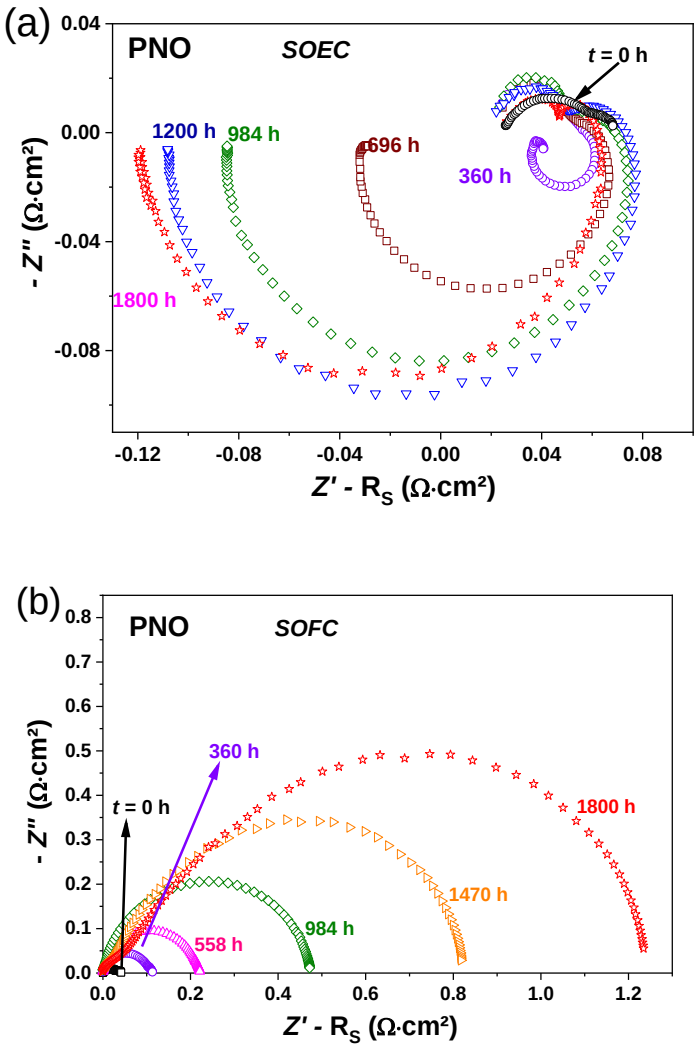


Fig. 4. Nyquist plots of PNO aged under $i_{dc}$ = 300 mA·cm$^{-2}$ at 700 °C up to 1800 h in (a) SOEC mode and (b) SOFC mode.

An inductive loop on one side of the cell (here the SOEC side) has a corresponding positive R//CPE contribution on the other side (the SOFC side), which is convoluted with the electrode impedance

response, virtually increasing the value of the polarization resistance. When measuring the whole cell (SOEC + SOFC), this artifact does not appear because addition of the inductive loop and the R//CPE cancel each other.

The way of fitting of the artifact is described in Fig. 5, from impedance data obtained with PNO after 1200 h of ageing at 700 °C as an example. First, the artifact is fitted based on the inductive tail, here on the SOEC impedance diagram, using a negative R//CPE (Fig. 5a). The fit is completed using a series resistance, a R//CPE for the oxide oxidation reaction (OOR) at the SOEC electrode, and a finite length Warburg for the gas diffusion [50].

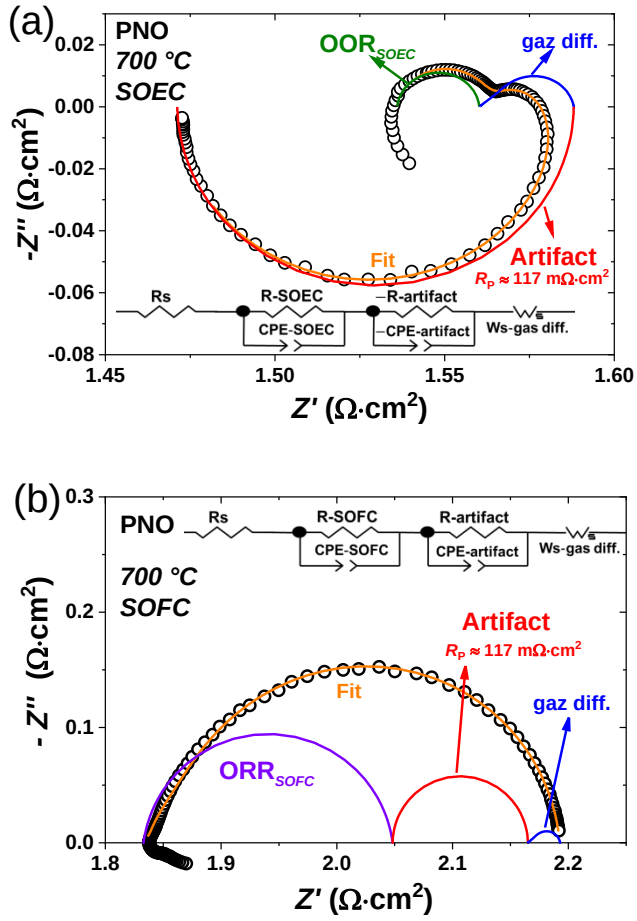

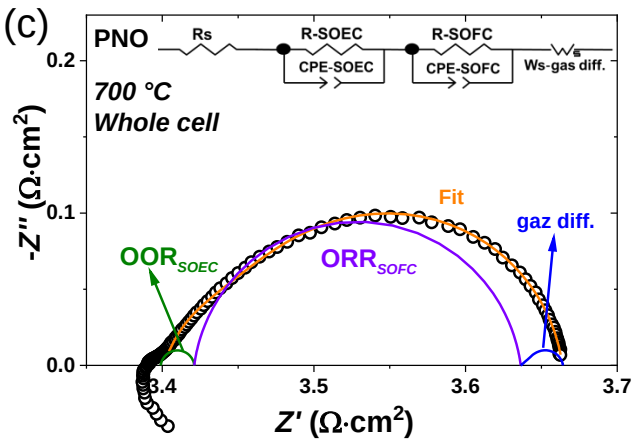


Fig. 5. Impedance diagrams of PNO recorded after 1200 h of ageing at 700 °C as an example: (a) SOEC side; (b) SOFC side; (c) whole cell. The artifact is identified as an inductive loop at the SOEC side (a), together with the $OOR_{SOEC}$ arc; (b) at the SOFC side, the $ORR_{SOFC}$ arc is calculated taking into account this artifact. (c) Combination of the $OOR_{SOEC}$ and $ORR_{SOFC}$ arcs results in the whole cell impedance.

Table 1. Fitting results of impedance data analysis for PNO symmetrical half-cell.

| | $R_S$ (Ω·cm²) | ORR/OER | | | Artifact | | | Gas diffusion Warburg short (*Ws*) | | |
|---|---|---|---|---|---|---|---|---|---|---|
| | | *R* (Ω·cm²) | CPE (F) | *n* | *R* (Ω·cm²) | CPE (F) | *n* | *Ws* (R) (Ω·cm²) | *Ws* (CPE) (F) | *Ws* (*n*) |
| SOFC | 1.84 | 0.215 | 0.24 | 0.9 | 0.117 | 0.42 | 1 | 0.028 | 1.7E-2 | 0.5 |
| SOEC | 1.535 | 0.025 | 9.2E-4 | 0.99 | 0.117 | - 0.42 | 1 | 0.028 | 7.7E-3 | 0.44 |

The values obtained for the artifact and the gas diffusion are kept for fitting the SOFC impedance diagram (Fig. 5b). An additional R//CPE arc is added to complete the fit, which represents the oxygen reduction reaction (ORR) at the SOFC electrode. The results of the fitted impedance data are summarized in Table 1.

The artifact does not appear on the total impedance diagram (Fig. 5c), which can be fitted using the ORR from the SOFC side, the OOR from the SOEC side and the gas diffusion. Only the OOR and the ORR are considered for calculating the polarization resistance.

Upon treatment of the artifact, the polarization resistance of PNO is found stable in SOEC mode after 1800 h at 700 °C (close to 0% degradation, Fig. 4a). Only the inductive loop increases with the ageing time. On the other hand, $R_P$ significantly increases in SOFC mode (+ 3350% after 1800 h, Fig. 4b).

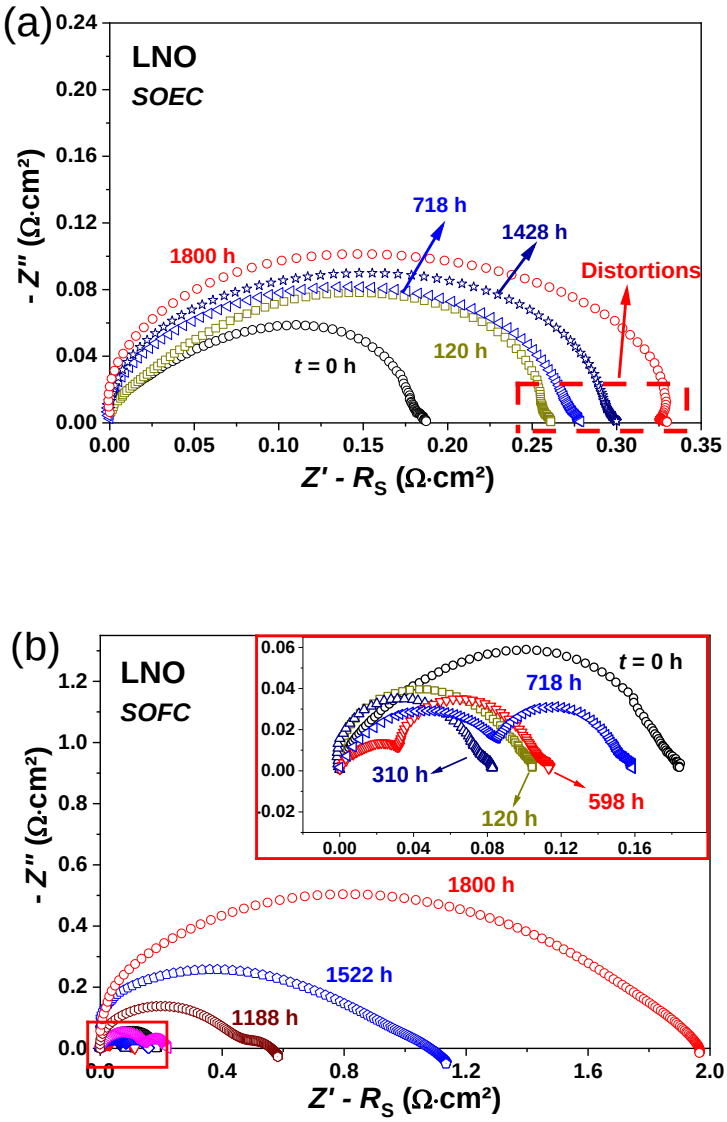


Fig. 6. Nyquist plots of LNO aged at 700 °C, up to 1800 h under $i_{dc}$ = 300 mA·cm$^{-2}$ in (a) SOEC mode, and (b) SOFC mode.

The results for LNO are reported in Fig. 6. Distortions of the impedance diagrams appear after 700 h, but their effects are negligible on the ORR/OOR impedance arcs (cf. detail in Fig. 6a). In SOFC

mode, the electrochemical polarization resistance of LNO drastically increases from $R_p$ = 0.18 Ω·cm$^2$ initially up to roughly 2 Ω·cm$^2$ after 1800 h (+1110 %). In SOEC mode, the increase is less pronounced, $R_p$ reaching 0.33 Ω·cm$^2$ after 1800 h (+180 %).

Finally, the results for LP5NO are given in Fig. 7. An inductive loop again appears in SOEC mode, but to a lesser extent than for PNO. The oxygen electrode deteriorates more significantly in SOFC mode (+350%) than in SOEC mode (close to 0%).

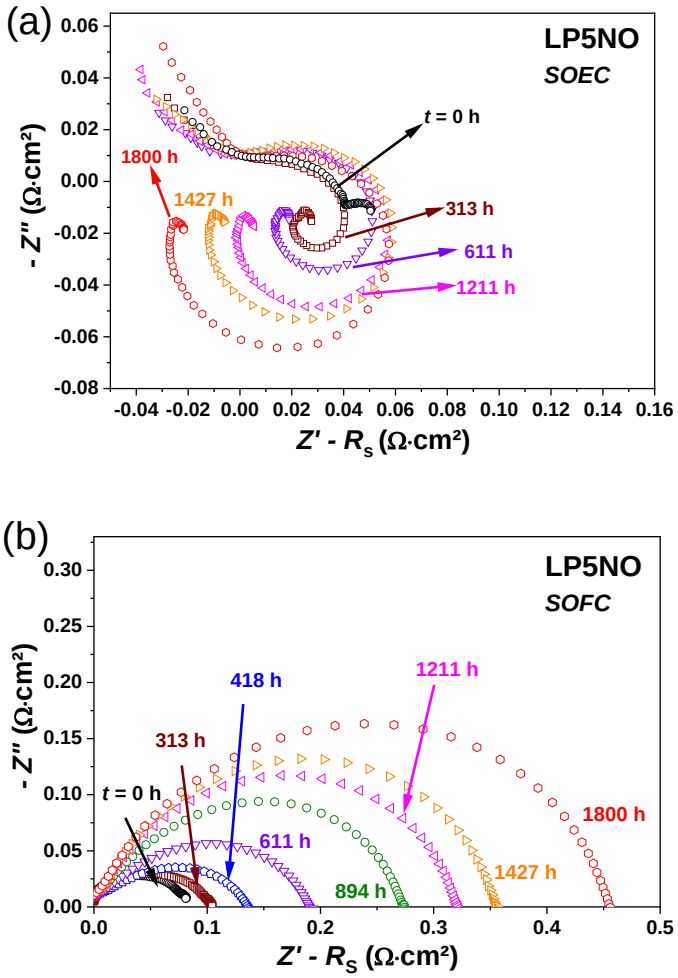


Fig. 7. Nyquist plots of LP5NO aged at 700 °C, up to 1800 h, under $i_{dc}$ = 300 mA·cm$^{-2}$ in (a) SOEC mode and (b) SOFC mode.

The time dependence of the additional polarization resistance $\Delta R_P = R_{Pgt} - R_{Pini}$ ($R_{Pini}$ and $R_{Pgt}$ being the polarization resistances at $t$ = 0 and at a given time, respectively) is summed up for the three

electrodes in Fig. 8, in both SOEC and SOFC modes. In SOEC mode, the polarization resistances of PNO and LP5NO are stable, while that of LNO slightly increases. In SOFC mode, the sample suffering the highest degradation is LNO, then PNO and LP5NO. These degradations are far higher than those observed in SOEC mode.

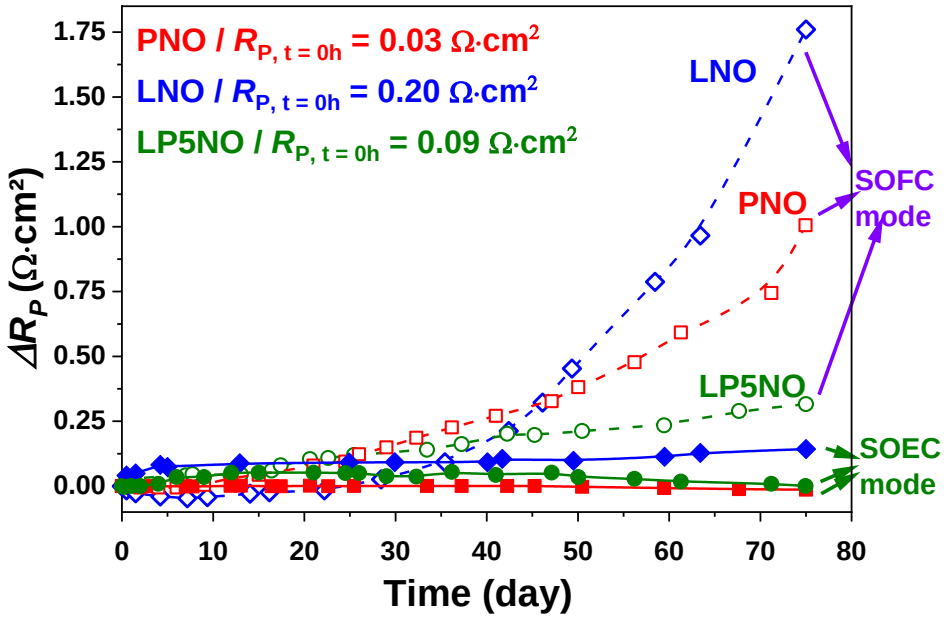


**Fig. 8.** Additional polarization resistance $\Delta R_P$ for PNO, LNO and LP5NO vs. time during ageing at 700 °C, $i_{dc}$ = 300 mA·cm$^{-2}$, in SOFC or SOEC mode.

In addition, the variation of series resistance ($R_s$) were also investigated for all three cells under both SOFC and SOEC mode and depicted in supplementary information Fig. S1. Slight difference in $R_s$ for SOFC and SOEC mode may be due to some difference between the interfaces i.e. electrode//GDC$_{BL}$ and GDC$_{BL}$//YSZ on both sides of the half-cell (also might be due to the slight differences in area of GDC or electrode, non-symmetrical electrode, or non-perfect polishing of the surface for instance). A continuous increase in $R_s$ is observed in SOFC mode but remarkably it is stable under SOEC mode for all three cells. However the extent of increase in $R_s$ in SOFC mode is

different for all three cells. LNO cell shows the largest increase in $R_s$ (0.4 Ω·cm$^2$ after 1800 h) then the PNO (0.17 Ω·cm$^2$ after 1800 h) and LP5NO (0.06 Ω·cm$^2$ after 1800 h).

In the last part, the origin of these degradations is discussed.

### *3.3. Origin of the degradations of LNO, PNO and LP5NO electrochemical performances during ageing under polarization*

#### *3.3.1. Post-mortem X-ray diffraction analyses*

After the ageing experiments, the top surface of the electrodes was analyzed using X-ray diffraction. PNO totally decomposes into $Pr_6O_{11}$, in addition with $Pr_4Ni_3O_{10+\delta}$ and NiO on the SOFC side, or $PrNiO_{3-\delta}$ on the SOEC side. Slight decomposition of LNO and LPNO into $Ln_4Ni_3O_{10\pm\delta}$ and $La_2O_3$ occurs, but the extent of the decomposition is comparable in SOEC and SOFC modes and cannot account for the differences in electrochemical performances. The lanthanide nickelate electrodes, $GDC_{BL}$ and 8YSZ electrolytes are excellent SOFC/SOEC materials on their own; then, issues with their electrochemical performances most probably come from reactivity at their interfaces when stacked and exposed to high temperature [24, 47, 51].

#### *3.3.2. Post-mortem FIB-SEM analysis*

FIB-SEM micrographs of the three electrodes after the ageing experiments were performed on both SOEC and SOFC sides. The results for LNO are presented in Fig. 9.

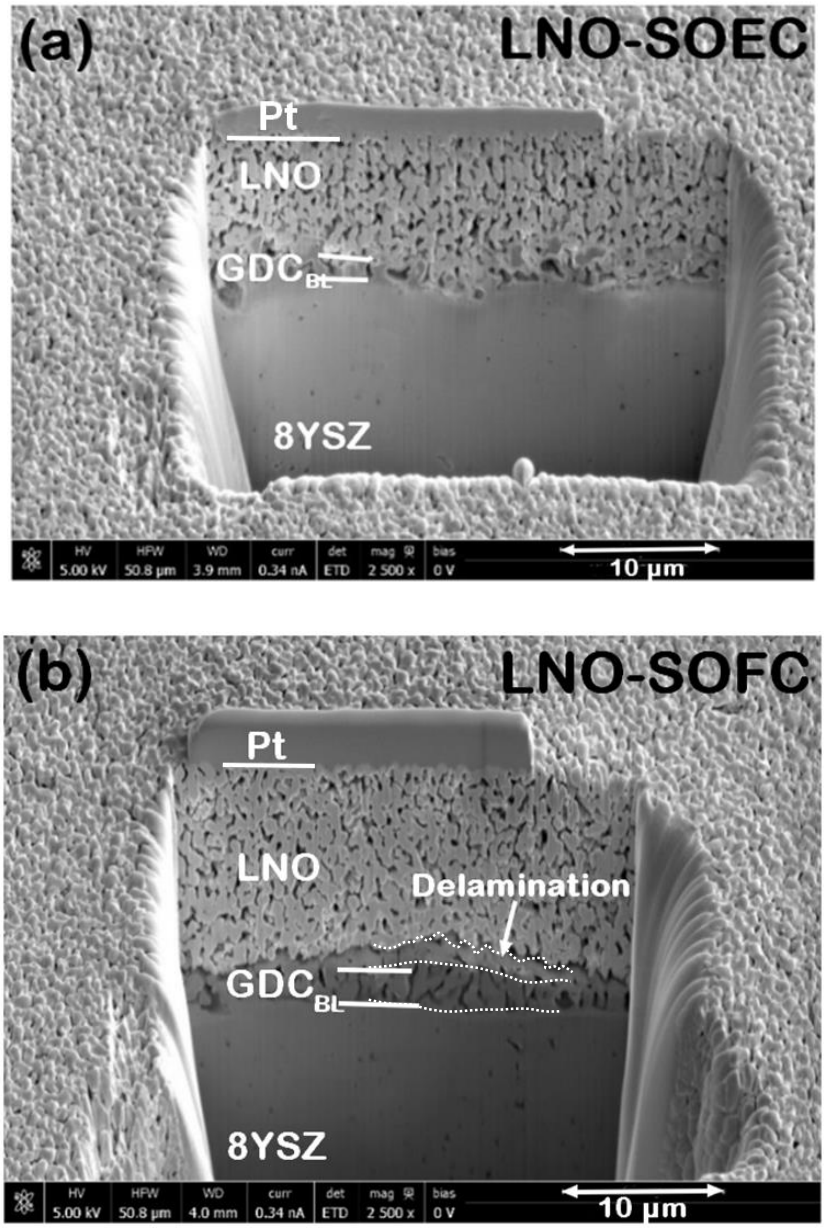


Fig. 9. FIB-SEM micrographs of LNO//$GDC_{BL}$//8YSZ after 1800 h of ageing at 700 °C. (a) SOEC side, (b) SOFC side.

Looking at the micrographs of the electrodes, the interfaces between LNO//$GDC_{BL}$ and $GDC_{BL}$//8YSZ seem rather good in SOEC mode (hence, no increase in $R_s$ is observed under SOEC mode), which may explain the good ageing results. Conversely, partial delamination between LNO and $GDC_{BL}$ occurs on the SOFC side which could be responsible for the degradation of the

electrochemical performances. This partial delamination further explains the increase in $R_s$ in SOFC mode (supplementary information Fig S1c).

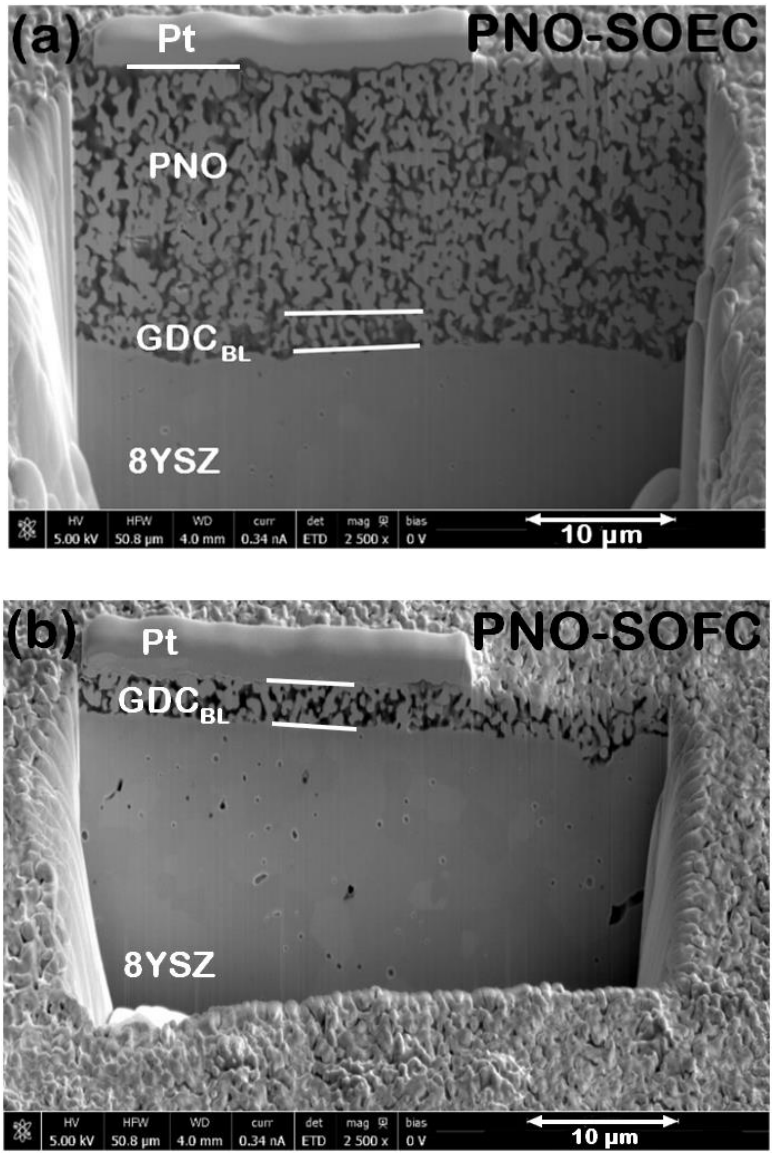


Fig. 10. FIB-SEM micrographs of PNO//GDC$_{BL}$//8YSZ after 1800 h of ageing at 700 °C. (a) SOEC side, (b) SOFC side.

The PNO electrode (Fig. 10) delaminated on the SOFC side upon removal of the half-cell from the EIS setup, which explains that only GDC and 8YSZ are present in Fig. 10(b) and again a increase

in $R_s$ was observed (supplementary information Fig S1a). In contrast, the morphology of the half-cell on the SOEC side is quite good. These observations are very similar to those made for LNO and lead to the same conclusion concerning the ageing behaviors.

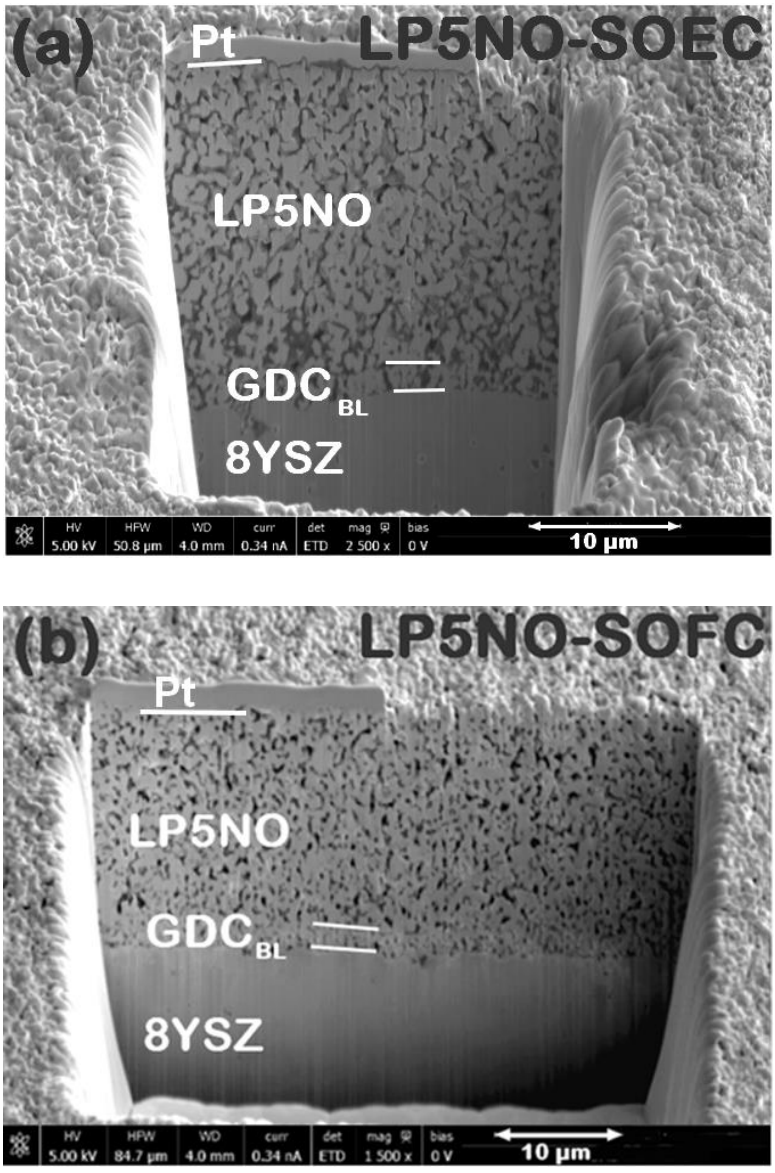


Fig. 11. FIB-SEM micrographs of LP5NO//$GDC_{BL}$//8YSZ after 1800 h of ageing at 700 °C. (a) SOEC side, (b) SOFC side.

Micrographs of LP5NO are shown in Fig. 11. Surprisingly, no delamination occurs on the SOFC side, nor on the SOEC side.

The good performances obtained with LP5NO in SOFC mode, compared to LNO or PNO, may be explained by this absence of delamination, as almost stable Rs value is observed (supplementary information Fig S1b). But the differences in ageing of LP5NO either in SOFC or SOEC mode are hardly explained by the micrographs. The authors are convinced that the reactivity at the LPNO//$GDC_{BL}$ interfaces differs during the ageing, depending on how the electrode operates in SOFC or SOEC mode.

To corroborate these results and assumption, EDX line-scan analyses of the electrodes have been tentatively carried out from the electrode toward the electrolyte. Unfortunately, the results are inconclusive, which likely means that the differences are subtle; more studies would be required to be distinguished.

### *3.4. Comparison of the LPNO electrodes with classical perovskite materials*

Many ageing studies about SOEC/SOFC complete cells containing perovskite electrodes as for instance LSM [52-54] or LSCF [55] have been published. All of them conclude that the main degradation occurs at the oxygen electrode concerned with the perovskite materials. In SOEC mode, the degradations are related to an over-concentration of oxygen species at the oxygen electrode//electrolyte interface, which progressively forms bubbles, ultimately leading to delamination. The migration of cations from the oxygen electrode//electrolyte interface toward the hydrogen electrode//electrolyte could also explain the delamination [56]. In SOFC mode, no clear microstructural features explain the degradations, which are usually attributed to Sr enrichment at the electrode//electrolyte interface.

It is noteworthy that we observed the opposite trend for the lanthanide nickelate, the oxygen electrode working in SOEC being highly stable, while the SOFC one delaminates. The delamination at the SOFC side may occur due to insufficient oxygen supply at the electrode //electrolyte interface: indeed, the EIS setup does not allow forcing a gas flow inside the porosity of the electrode. Hence, the degradation on the SOFC side could be lessened, or even removed using an optimized setup.

On the other hand, the higher stability of the lanthanide nickelates with respect to the perovskite materials in SOEC is likely due to a significant difference in the ionic conductivity mechanism. For the lanthanide nickelates, it results from their oxygen over-stoichiometry (i.e. additional oxide ions in the network), while it arises from oxygen vacancies for the perovskites.

In the SOEC conditions, a large inflow of oxide ions takes place from the electrolyte toward the electrode, which decreases the under-stoichiometry of the perovskite inducing a decrease of their electrochemical performances. It is the contrary for the lanthanide nickelates that are able to insert additional oxide ions. This might explain the over-concentration of oxygen species occurring at the perovskite electrode//electrolyte interface working in SOEC, leading to delamination, while no such issues are observed in the current study for the lanthanide nickelates.

The next step will be to confirm the performances and ageing capability of the lanthanide nickelate in a real SOEC setup.

## 4. Conclusions

This study reported the ageing behaviour of electrodes of $La_2NiO_{4+\delta}$, $Pr_2NiO_{4+\delta}$, and their mixed products $La_{2-x}Pr_xNiO_{4+\delta}$, with $x$ = 0.5, 1 and 1.5, with or without polarization, at 700 °C. These materials were screen printed on dense ceramics of 8YSZ coated with a thin barrier layer of GDC.

First, the chemical stability of the raw powders was studied at 600 °C, 700 °C, and 800 °C. LNO was quite stable whatever the temperature, while PNO decomposed into a mixture of $Pr_6O_{11}$, $PrNiO_{3-\delta}$, $Pr_4Ni_3O_{10+\delta}$ and NiO as previously reported. Among the LPNO materials, the $x$ = 0.5 composition (LP5NO) was chemically as stable as LNO, the ones with $x$ = 1 or 1.5 (LP10NO or LP15NO) decomposing as their parent phase PNO.

The electrochemical stability of all these materials as oxygen electrode was rather good without polarization over one month. A comparatively large increase in the polarization resistance of LNO and PNO occurred, while all the LPNO compounds were stable.

However, under polarization ($i_{dc}$ = 300 mA·cm$^{-2}$), PNO, LNO and LP5NO significantly damaged when working in SOFC conditions, i.e. in oxygen reduction reaction, in the $R_P$ order LNO > PNO > LP5NO. Delamination occurred at the interface between LNO or PNO and $GDC_{BL}$, which was believed to come from a poor supply of oxygen inside the porosity of the electrode, toward the active sites for the oxygen reduction reaction. This delamination accounted for the increase of the polarization resistance of both electrodes. No delamination was observed for LP5NO, which may explain its better final performances than LNO or PNO. In that case, the degradations may come from a progressive reactivity at the interfaces between LP5NO and GDC, but no proof could be provided by XRD or FIB-SEM analyses.

The behaviour of these electrodes in SOEC conditions, i.e. for the oxide ion oxidation reaction, was remarkable. If a slight increase of the polarization resistance was measured for LNO (+ 0.14 Ω·cm$^2$ after 1800 h), the polarization resistances of PNO and LP5NO were stable at respectively 0.03 Ω·cm$^2$ and 0.09 Ω·cm$^2$ at 700 °C for 1800 h. In addition, no delamination was observed in contrast with previous reports on LSC or LSCF. These results are very promising for the development of an efficient and durable solid oxide electrolysis cell.

**Acknowledgments**

This work was performed under PEREN project (reference: ANR-2011-PREG-016-05). The authors wish to gratefully acknowledge the Agence Nationale de la Recherche (A.N.R., France) for supporting these scientific works and for the financial support.

**References**

[1] R. Knibbe, A. Hauch, J. Hjelm, D. Ebbesen Sune, M. Mogensen, Durability of Solid Oxide Cells, in: Green, 2011, pp. 141.
[2] H. Yokokawa, H. Tu, B. Iwanschitz, A. Mai, Journal of Power Sources, 182 (2008) 400-412.
[3] R.E. van Doorn, I.C. Fullarton, R.A. de Souza, J.A. Kilner, H.J.M. Bouwmeester, A.J. Burggraaf, Solid State Ionics, 96 (1997) 1-7.
[4] G.C. Kostogloudis, C. Ftikos, Solid State Ionics, 126 (1999) 143-151.
[5] V.V. Kharton, A.P. Viskup, D.M. Bochkov, E.N. Naumovich, O.P. Reut, Solid State Ionics, 110 (1998) 61-68.
[6] A.J. Jacobson, Chemistry of Materials, 22 (2010) 660-674.
[7] A. Petric, P. Huang, F. Tietz, Solid State Ionics, 135 (2000) 719-725.
[8] M.Y. Lu, J.G. Railsback, H. Wang, Q. Liu, Y.A. Chart, S.-L. Zhang, S.A. Barnett, Journal of Materials Chemistry A, 7 (2019) 13531-13539.
[9] M.-B. Choi, B. Singh, E.D. Wachsman, S.-J. Song, Journal of Power Sources, 239 (2013) 361-373.
[10] V.C. Kournoutis, F. Tietz, S. Bebelis, Fuel Cells, 9 (2009) 852-860.
[11] M. Søgaard, P.V. Hendriksen, M. Mogensen, F.W. Poulsen, E. Skou, Solid State Ionics, 177 (2006) 3285-3296.
[12] J. Januschewsky, M. Ahrens, A. Opitz, F. Kubel, J. Fleig, Advanced Functional Materials, 19 (2009) 3151-3156.
[13] K. Kurata, Y. Toyota, T. Sato, E. Niwa, K. Shozugawa, M. Matsuo, T. Hashimoto, Journal of the Ceramic Society of Japan, 125 (2017) 227-235.
[14] Y. Bo, Z. Wenqiang, X. Jingming, C. Jing, International Journal of Hydrogen Energy, 33 (2008) 6873-6877.
[15] S. Sun, Z. Cheng, Journal of The Electrochemical Society, 164 (2017) F3104-F3113.
[16] G.C. Kostogloudis, G. Tsiniarakis, C. Ftikos, Solid State Ionics, 135 (2000) 529-535.
[17] D. Oh, D. Gostovic, E.D. Wachsman, Journal of Materials Research, 27 (2012) 1992-1999.
[18] F. Wang, K. Yamaji, D.-H. Cho, T. Shimonosono, H. Kishimoto, M.E. Brito, T. Horita, H. Yokokawa, Solid State Ionics, 225 (2012) 157-160.
[19] V. Vibhu, S. Yildiz, I.C. Vinke, R.-A. Eichel, J.-M. Bassat, L.G.J. de Haart, Journal of The Electrochemical Society, 166 (2019) F102-F108.
[20] S.J. Kim, G.M. Choi, Solid State Ionics, 262 (2014) 303-306.
[21] F. Wang, T. Nakamura, K. Yashiro, J. Mizusaki, K. Amezawa, Physical Chemistry Chemical Physics, 16 (2014) 7307-7314.
[22] G. Amow, I.J. Davidson, S.J. Skinner, Solid State Ionics, 177 (2006) 1205-1210.

[23] S. Takahashi, S. Nishimoto, M. Matsuda, M. Miyake, Journal of the American Ceramic Society, 93 (2010) 2329-2333.
[24] R. Sayers, J. Liu, B. Rustumji, S.J. Skinner, Fuel Cells, 8 (2008) 338-343.
[25] Y. Nigara, P. Odier, A.M. Anthony, Science of Ceramics 11, The Swedish Sot. Ceramics,, 11 (1981) 551-557.
[26] J.M. Bassat, P. Odier, J.P. Loup, Journal of Solid State Chemistry, 110 (1994) 124-135.
[27] V. V. Kharton, A. P. Viskup, E. N. Naumovich, F. M. B. Marques, Journal of Materials Chemistry, 9 (1999) 2623-2629.
[28] S.J. Skinner, J.A. Kilner, Solid State Ionics, 135 (2000) 709-712.
[29] E. Boehm, J.M. Bassat, P. Dordor, F. Mauvy, J.C. Grenier, P. Stevens, Solid State Ionics, 176 (2005) 2717-2725.
[30] J.-M. Bassat, V. Vibhu, C. Nicollet, A. Flura, S. Fourcade, J.-C. Grenier, A. Rougier, ECS Transactions, 78 (2017) 655-665.
[31] V. Vibhu, A. Rougier, C. Nicollet, A. Flura, S. Fourcade, N. Penin, J.-C. Grenier, J.-M. Bassat, Journal of Power Sources, 317 (2016) 184-193.
[32] C. Ferchaud, J.-C. Grenier, Y. Zhang-Steenwinkel, M.M.A. van Tuel, F.P.F. van Berkel, J.-M. Bassat, Journal of Power Sources, 196 (2011) 1872-1879.
[33] M.A. Laguna-Bercero, H. Monzón, A. Larrea, V.M. Orera, Journal of Materials Chemistry A, 4 (2016) 1446-1453.
[34] X. Tong, F. Zhou, S. Yang, S. Zhong, M. Wei, Y. Liu, Ceramics International, (2017).
[35] C. Zhao, Q. Zhou, T. Zhang, L. Qu, X. Yang, T. Wei, Materials Research Bulletin, 113 (2019) 25-30.
[36] A. Flura, S. Dru, C. Nicollet, S. Fourcade, A. Rougier, J.M. Bassat, J.C. Grenier, 5th International Conference on Fundamentals and Development of Fuel Cells "FDFC 2013", (2013).
[37] V. Vibhu, A. Rougier, C. Nicollet, A. Flura, J.-C. Grenier, J.-M. Bassat, Solid State Ionics, 278 (2015) 32-37.
[38] V. Vibhu, I.C. Vinke, R.-A. Eichel, J.-M. Bassat, L.G.J. de Haart, ECS Transactions, 91 (2019) 1327-1339.
[39] S.J. Kim, K.J. Kim, A.M. Dayaghi, G.M. Choi, International Journal of Hydrogen Energy, 41 (2016) 14498-14506.
[40] P. Courty, H. Ajot, C. Marcilly, B. Delmon, Powder Technology, 7 (1973) 21-38.
[41] A.D. Rougier, A. Flura, C. Nicollet, V. Vibhu, S. Fourcade, E. Lebraud, J.-M. Bassat, J.-C. Grenier, ECS Transactions, 68 (2015) 817-823.
[42] S.B. Adler, Journal of The Electrochemical Society, 149 (2002) E166-E172.
[43] S.B. Adler, B.T. Henderson, M.A. Wilson, D.M. Taylor, R.E. Richards, Solid State Ionics, 134 (2000) 35-42.
[44] J. Winkler, P.V. Hendriksen, N. Bonanos, M. Mogensen, Journal of The Electrochemical Society, 145 (1998) 1184-1192.
[45] A. Flura, S. Dru, C. Nicollet, V. Vibhu, S. Fourcade, E. Lebraud, A. Rougier, J.-M. Bassat, J.-C. Grenier, Journal of Solid State Chemistry, 228 (2015) 189-198.
[46] V. Vibhu, A. Flura, C. Nicollet, S. Fourcade, N. Penin, J.-M. Bassat, J.-C. Grenier, A. Rougier, M. Pouchard, Solid State Sciences, 81 (2018) 26-31.
[47] A. Flura, C. Nicollet, V. Vibhu, B. Zeimetz, A. Rougier, J.-M. Bassat, J.-C. Grenier, Journal of The Electrochemical Society, 163 (2016) F523-F532.
[48] M. Cimenti, A.C. Co, V.I. Birss, J.M. Hill, Fuel Cells, 7 (2007) 364-376.
[49] M. Cimenti, V.I. Birss, J.M. Hill, Fuel Cells, 7 (2007) 377-391.
[50] A. Flura, C. Nicollet, S. Fourcade, V. Vibhu, A. Rougier, J.M. Bassat, J.C. Grenier, Electrochimica Acta, 174 (2015) 1030-1040.

[51] A. Montenegro-Hernández, A. Soldati, L. Mogni, H. Troiani, A. Schreiber, F. Soldera, A. Caneiro, Journal of Power Sources, 265 (2014) 6-13.
[52] C. Graves, S.D. Ebbesen, S.H. Jensen, S.B. Simonsen, M.B. Mogensen, Nat Mater, 14 (2015) 239-244.
[53] M.J. Heneka, E. Ivers-Tiffée, ECS Proceedings Volumes, 2005-07 (2005) 534-543.
[54] A.V. Virkar, J. Nachlas, A.V. Joshi, J. Diamond, Journal of the American Ceramic Society, 73 (1990) 3382-3390.
[55] S.P. Simner, M.D. Anderson, M.H. Engelhard, J.W. Stevenson, Electrochemical and Solid-State Letters, 9 (2006) A478-A481.
[56] G. Petot-Ervas, C. Petot, J.M. Raulot, J. Kusinski, Defect and Diffusion Forum, 237-240 (2005) 843-848.

## Graphical Abstract

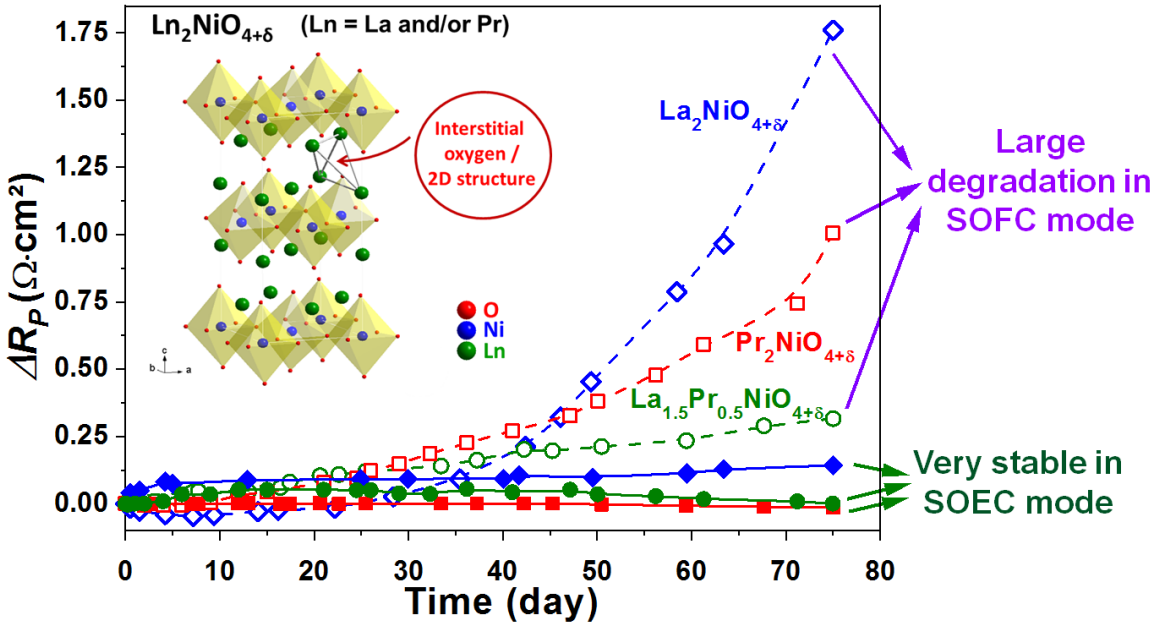


Description (20-35 words): The investigations of Lanthanide nickelates as oxygen electrodes for solid oxide cells show a large degradation in SOFC mode while a very stable behaviour in SOFC mode.